communications biology

Article

https://doi.org/10.1038/s42003-025-07573-3

Multiple kinesins speed up cargo transport in crowded environments by sharing load

Check for updates

Ya-Ting Huang[1], Michio Tomishige[2], Steven P Gross[3], Pik-Yin Lai[1,4] ✉ & Yonggun Jun[1] ✉

Kinesin motors transport cargoes along microtubules inside of cells. Although it is well known that the cargoes are typically carried by multiple kinesins and that the more motors used, the further the cargoes travel, it has been challenging to determine the number of motors moving a cargo and any instant. Further, there is no unified statement on the relationship between cargo velocity and motor number, especially in the presence of a very crowded cytoplasmic environment. Here, we use a non-invasive method to quantify instantaneous motor number, and use it to investigate the effects of crowded environments on cargo motion when it is carried by multiple kinesins. Our experiments reveal that the velocity of the cargo depends on the number of motors on the cargo and the size of the crowders in crowded environments. Our finding suggests that kinesin tension plays a role in collective motion, which has been confirmed through stochastic kinesin simulations. Overall, our study demonstrates the broad applicability of the non-invasive method to determine engaged motor numbers and sheds light on the intriguing interplay between macromolecular crowding, kinesin tension, and kinesin-mediated cargo transport.

Eukaryotic cells rely on intracellular transport for proper functioning. The movement of cargoes is a critical aspect of this cellular traffic and is facilitated by molecular motors such as kinesin[1–3]. The kinesin motors exhibit processive movement, fueled by ATP hydrolysis, taking repeated 8-nanometer steps toward the cell's periphery[4]. They work in teams to deliver the cellular cargo further and to overcome obstacles that can block cargo advance[5–7]. Numerous in vitro experiments have been conducted using a DNA scaffold or an antibody to investigate this collective motion[8–10] and have found that cargo velocities are constant regardless of the number of engaged kinesin motors. However, this finding contradicts the diverse velocity distributions observed in cells. Despite extensive studies of the motors' behavior in simplified, low-viscosity environments, understanding their true function within complex and crowded cellular environments remains a challenge.

A key feature of the interior of cells is the presence of macromolecular crowding, where 30-40% of the cell volume can be taken up by macromolecules and small compounds, creating a highly structured environment[11,12]. This phenomenon has pronounced effects on various biochemical processes, including changes in association rates and enzymatic activity[13,14]. Intracellular trafficking is also influenced by macromolecular crowding[5,6,15–17]. In vitro experiments have been employed to investigate the influence of macromolecular crowding agents on cargo transport by kinesin motors[18–21]. For a single kinesin, crowding agents are small molecules or proteins that hinder movement. However, for transport by multiple motors, two research groups studying the process disagreed as far as cargo velocity in different crowded environments. The velocity of the cargo was reported to decrease with multiple kinesins in the crowded BSA solution[21] but was also reported to stay constant regardless of the number of motors in the dextran-Ficoll solution[18]. Finally, it was reported to gradually increase with the increasing number of kinesins in the crowded Xanthan gum solution[19].

Overall, we hypothesize that different environments lead to different velocities in cargo transport. To test this directly, we measured the velocity of the cargo with an unknown number of motors involved in transport in the solution of the various concentrations of crowders, such as Xanthan gum, BSA, and glycerol. We used the fluctuation theorem to identify the number of active motors. The results show that a single kinesin motor moving a bead slowed down in the presence of crowders of any size. However, multiple kinesin motors exhibited an increase in cargo velocity in the presence of large crowders. Motivated by these data, we performed a Langevin dynamics simulation and found that the stretching of the kinesin, and thus force on the cargo by the kinesins, is reduced for the transport by multiple motors in a very crowded environment.

[1]Department of Physics and Center for Complex Systems, National Central University, Taoyuan, 320, Taiwan. [2]Department of Physical Sciences, Aoyama Gakuin University, 252-5258 Kanagawa, Japan. [3]Developmental and Cell Biology, University of California, Irvine, CA, 92697, USA. [4]Physics Division, National Center for Theoretical Sciences, Taipei, 10617, Taiwan. ✉e-mail: pylai@phy.ncu.edu.tw; yonggun@phy.ncu.edu.tw

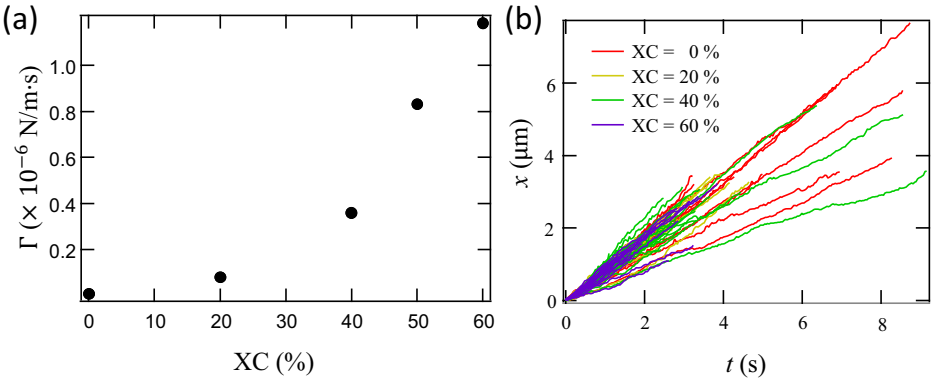

Fig. 1 | Friction coefficients, Γ and cargo motion in various XCs. a The friction coefficients measured in various xanthan concentrations. **b** Trajectories of cargo in different concentrations of xanthan solution. (red: 0% XC, orange: 20% XC, green: 40% XC, and purple: 60% XC), respectively. For 60% Xanthan Concentration (XC), the drag coefficient Γ is more than a hundred times higher than that of XC = 0%, which is large enough to check the effect of crowders on kinesin velocity.

Results

Velocity distribution of cargoes dragged by multiple motors

Kinesin bead assay experiments and data analysis were carried out as previously described[22]. Briefly, experiments were performed in the flow channel, whose inner surface is coated with microtubules (MT). The bead-to-kinesin ratio (the number of kinesins tethered on a bead) was properly adjusted, but the number of motors on a specific bead is unknown. To find out why the cargo velocity in-vivo is broadly distributed compared to that in vitro[5,6,15–17], we first increased the complexity of the kinesin assay buffer (KAB) using Xanthan gum polymer as crowders. We controlled the concentrations of Xanthan in the kinesin assay buffer (XKAB) to study the effect of crowder concentration on cargo velocity. We first prepared the master Xanthan solution and then diluted it from 20% to 60%[19]. The degree of crowdedness is determined not only by the concentration but also drag coefficient, Γ. The latter was obtained from the mean square displacement method based on the free-diffusion trajectories of the tracers. (Fig. 1a). The maximum Γ is about 1.18×10^{-3} pN/nm · s, which is 140 times higher than the 0% xanthan solution and large enough to check the effect of viscosity on the velocity of the cargo.

When a particle with kinesins is brought to the MT using optical tweezers, the kinesins bind to the MT and move linearly along the MT because of the processivity of kinesins. As shown in Fig. 1b, the cargoes move a long distance with multiple kinesins, which agrees well with previous studies[8–10] that multiple kinesins are one of the factors causing the long run length. For the further analysis, we dropped the trajectories whose velocity is less than 200 nm/s.

Identification of the number of motors involved in cargo transport

As described above, the wide distribution of cargo velocity is well-known to be due to the collective motion of multiple motors[19]. However, in general, it is difficult to identify the number of motors, N, actively involved in cargo transport. For this, some studies have used optical tweezers to measure the force of cargo hauled by motors[22], but this does not provide the value of N during cargo transport. Recently, a non-invasive technique using the fluctuation theorem (FT) was implemented to identify the number of motors engaged in the cargo during transport[23–26]. FT relates the probability of observing forward and reverse fluctuations in a system to its thermodynamic properties, and for cargo motion, it can be rewritten as follows:

$$\frac{P(\Delta x_p)}{P(-\Delta x_p)} = \exp\left[\frac{F_m \Delta x_p}{k_B T}\right], \tag{1}$$

where $\Delta x_p(\Delta t) = x_p(t+\Delta t) - x_p(t)$ is the displacement of cargo at the given time duration Δt, F_m is the force on cargo by motors, k_B is the Boltzmann constant, and T is a temperature. From Eq. (1), we define the degree of fluctuation χ:

$$\frac{F_m}{k_B T} = \ln\left[\frac{P(\Delta x_p)}{P(-\Delta x_p)}\right] / \Delta x_p \equiv \chi. \tag{2}$$

where χ is a function of Δt and represents the level of less fluctuation on a given time scale.

To determine $P(\Delta x_p)$ at the given time Δt, let us consider a single cargo trajectory, as shown in Fig. 2a. To determine the mean velocity, we performed a linear fit (brown line) on the cargo trajectory (black line). Inset shows the fluctuating nature of cargo motion during transport. From this, we obtained $P(\Delta x_p)$ (symbols) at Δt=190 ms, 380 ms, and 760 ms, as shown in Fig. 2b. When $P(\Delta x_p)$ are good approximations of the Gaussian distributions (solid lines), χ can be rewritten as $\chi = 2\mu/\sigma^2$ where $\mu = \langle \Delta x_p \rangle$ is the mean value and $\sigma^2 = \langle \Delta x_p^2 \rangle - \mu^2$ is the variance. Figure 2c of XC=40% shows that χ increases for a short time Δt, indicating that cargo fluctuations dominate. For a sufficiently large time interval (about ≥150 ms), χ converges to a constant, indicating that the ratio of mean velocity to velocity variance becomes saturated. In our data, about 65% of χ trajectories become constant, so the rest of them are dropped from further analysis. We took the average of a single trajectory of χ over saturated Δt to determine the saturated fluctuation unit, χ^*, in Fig. 2d. Due to the additivity of the kinesin force, the appearance of peaks in the histogram of χ at an integral multiple of around 0.1 (Fig. 2d) corresponds to a signature for the identification of the number of motors, which is in agreement with other experiments on kinesin[23] and dynein[26].

Kinesins share the load to move fast

Next, we determined the mean cargo velocity, $\langle v \rangle$, which is determined by averaging between $[0.1i - 0.05, 0.1i + 0.05]$ nm^{-1} (i is an integer), for different numbers of kinesins at different concentrations of XKAB. In 0% XKAB, $\langle v \rangle$ remains constant, 780 nm/s, regardless of the number of kinesins in the cargo, while the velocities of each cargo, v, are broadly distributed (Fig. 2e). In contrast, $\langle v \rangle$ in a 60% XKAB environment is approximately 700 nm/s for a single motor and gradually increases with increasing numbers of kinesins. (Fig. 2f). Figure 2g shows the average cargo velocities rescaled by the saturated velocity v_0 in various XKAB concentrations. For a single kinesin, cargo velocity becomes lower as the crowdedness increases, while the cargo velocity of more kinesins becomes higher and saturated, as shown in Fig. 2g. This can be explained by the shared-load model that states that the load on the cargo is evenly shared by each kinesin involved[19,27,28]. Hayashi et al. reported a similar trend in the transport of a synaptic vesicle precursor in axonal transport[23].

Furthermore, we investigated the effect of the size of the crowder molecules on cargo motion dragged by multiple kinesins. The sizes of the glycerol and BSA molecules are much smaller than that of Xanthan gum (185 nm), i.e., 1 nm and 3.62 nm, respectively[29–31]. We measured the mean speed of the cargo in the presence of smaller crowders. However, our finding indicates that cargo speeds slow down and are constant regardless of the concentrations of small crowders, such as BSA and glycerol (see Supplementary Fig. 1). When the assay buffer has smaller molecules, they directly interfere with the kinesin heads, causing significant changes to the stepping potential well, leading to a lower mean cargo velocity[21]. However, with larger molecules in the assay buffer, such as XKAB, the load is greater on the cargo, but there is no direct interference with individual kinesin motion. Therefore,

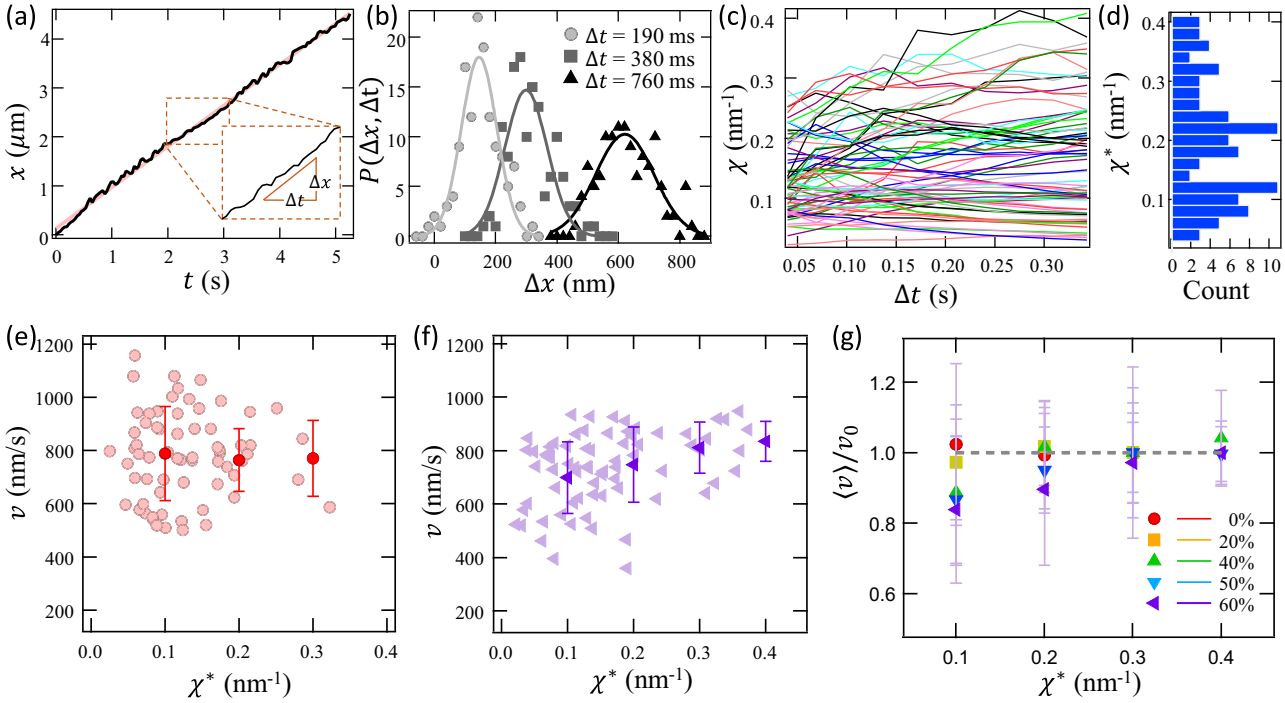

Fig. 2 | Cargo velocities dragged by multiple kinesins in various XCs. a Linear cargo trajectory. Insert: cargo displacement is defined as $\Delta x(t) = x(t + \Delta t) - x(\Delta t)$. **b** The PDFs of cargo displacement are getting wider with the increasing time interval. **c** The degree of fluctuation χ in time for XC=40%. **d** The histogram of χ^* is the saturated value of χ at the large time scale. Panels (**e**, **f**) are the individual (light colors) and the mean (dark colors) velocities in functions of χ^* for XC=0% and 60%, respectively. **g** The mean velocities of cargo rescaled by the velocity at XC=0% for various XCs. Error bars are the standard deviations. The total numbers of trajectories are 66, 51, 47, 73, and 72 from XC=0 to 60%, respectively.

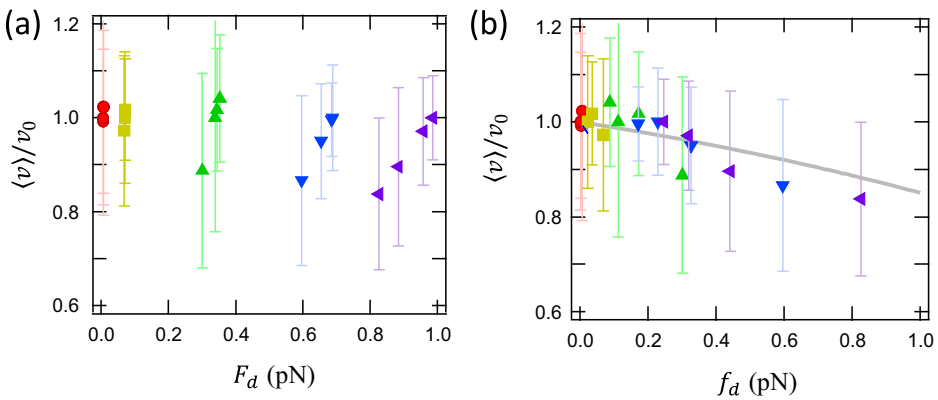

Fig. 3 | Mean velocities vs. drag force in various XCs. a The mean velocity as a function of the drag force F_d. It has the same symbols as Fig. 2g. **b** The mean velocity as a function of a single kinesin force f_d (the drag force F_d rescaled by N). The solid line is the theoretical line of the cargo velocity hauled by a single kinesin under the load based on the two-state model. Error bars are the standard deviations.

multiple kinesins work together to share the load on the cargo. This suggests that molecular size is also a factor that affects cargo velocity.

We also checked the relation between the average velocity of the cargo and the drag force, $F_d = \Gamma\langle v\rangle$ on cargo (see Fig. 3a). Moreover, when it is replotted in terms of the force, $f_d = F_d/N$, exerted by individual motors, all the points fall into a single curve (Fig. 3b). This is similar to the force-velocity relation determined by optical tweezers[32]. This suggests that kinesin motors work together to share the load and enable the cargo to move faster, particularly under high load conditions.

Numerical simulation of cargo motion

To further investigate the increase in velocity with increasing numbers of kinesins in crowded environments, we performed Langevin dynamics simulations based on the two-state kinetic model of kinesin movements[33–35], as shown in Fig. 4a. The transition rate from state 1 to state 2 is k_c, and the transition rates to make a forward or backward step in the stepping state are k_f and k_b, respectively. Here, k_f and k_b have an Arrhenius-type force dependency. The motor makes a forward or backward step of length d, and the cargo has a damping coefficient of Γ. Here, we consider that N motors are tethered to the cargo and attempt to move in the positive x direction. Let the instantaneous position of the cargo be $x_p(t)$, and let the head and tail positions of the j^{th} motor be denoted by $x_p(t) + \delta_j$ and $x_j(t)$, respectively (see Fig. 4b). The motor is attached to the particle by a spring of stiffness K_j. The intrinsic force-free size of the spring is denoted by ℓ_{oj}. The equations of motion are

$$\Gamma\dot{x}_p = -\sum_{j=1}^{N} K_j \Delta\ell_j + \xi_p(t), \tag{3}$$

where $\Delta\ell_j \equiv x_p + \delta_j + \ell_{oj} - x_j$ corresponds to the stretched length of the j^{th} kinesin, and ξ_p is white Gaussian thermal fluctuations that satisfy $\langle\xi_p\rangle = 0$ and $\langle\xi_p(t)\xi_p(t')\rangle = 2\Gamma k_B T\delta(t - t')$. The forward or backward rate $k_{f,b}^{(j)}$

depends on the force experienced by the motor and is modeled by the Bell's equation:

$$k_{f,b}^{(j)} = k_{0f,b}^{(j)} e^{\beta d_{f,b}^{(j)} K_j \Delta \ell_j}, \quad (4)$$

where $d_{f,b}^{(j)}$ are some characteristic distances.

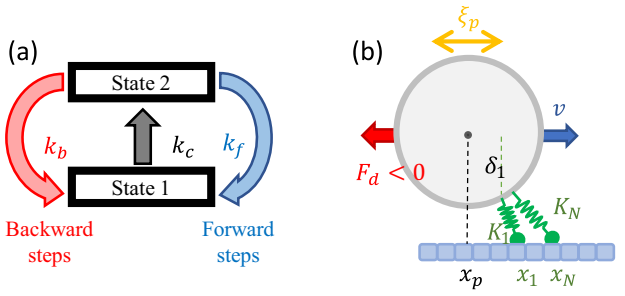

Fig. 4 | Schematic of the two-state model. a The two-state kinetic model for kinesin movement. The transition rate from the halt state to the stepping state is k_c, and the transition rates to make a forward or backward step in the stepping state are k_f and k_b, respectively. **b** The schematic of multiple motors (green) on a cargo (gray circle). N motors are tethered to the cargo and move in the positive x direction with the step of 8 nm. The instantaneous position of the cargo is $x_p(t)$, and the tail and head positions of the j^{th} motor are denoted by $x_p(t) + \delta_j$ and $x_j(t)$, respectively. When the cargo's velocity is v, the friction force $F_d = \Gamma v$ on the cargo is subject to a thermal force ξ_p.

The simulations were conducted with Langevin dynamics of the cargo, which is connected to the kinetic kinesin model via an elastic linker (Fig. 4b), using Eq. (14). The parameters used in the numerical simulation are taken from Ref. 35, such as k_c=1002s^{-1}, k_{0f}=102s^{-1}, k_{0b}=27.3s^{-1}. We also selected the stiffness of the kinesin stalk is 0.75×10^{-4} N/m, and the cargo radius is 250 nm. To verify the validity of our numerical simulation, we performed the simulation of cargo dragged by a single kinesin under the load. As shown in Supplementary Fig. 2, it is in good agreement with a theoretical model of the two-state model of kinesin steps[34,35].

Figure 5a shows the trajectories of the cargo carried by a single kinesin(s) for $\Gamma = 3 \times 10^{-5}$ pN/nm · s and $\Gamma = 3 \times 10^{-3}$ pN/nm · s, respectively. For the low Γ, the cargo fluctuates around the kinesin position, indicating that thermal force can overcome the viscous drag force, while cargo is always behind the kinesin for high Γ and moves slowly compared with the low Γ case. The cargo fluctuates less for the five motors hauling for low Γ, and the motor positions are everywhere around the cargo (Fig. 5b). For high Γ, however, all kinesins are stretched to pull the cargo. We then determined the cargo velocity by linear fitting the cargo trajectories. As shown in Fig. 5c, at low Γ, the mean velocity $\langle v \rangle$ is constant, which agrees well with the experimental results of Fig. 2e. At high Γ, the cargo pulled by a single motor moves slowly, increases, and asymptotically approaches v_0 with an increasing number of kinesins.

In Fig. 6a and b, we checked the kinesin stretching during transport, which cannot be obtained in real experiments. As the crowder concentration increases, the peak of the distribution for the length of a single kinesin moves to the right, indicating that the elastic force by the kinesin increases. For the case of multiple motors, the situation is similar, but the kinesin length for the high concentration is shorter than that of the low

Fig. 5 | Simulation of the cargo movement in various environments. Cargo trajectories hauled by a single kinesin (**a**) and five kinesins (**b**) for $\Gamma_1 = 3 \times 10^{-5}$ pN/nm · s and $\Gamma_4 = 3 \times 10^{-3}$ pN/nm · s. **c** Average cargo velocity with different numbers of kinesin involved in cargo transport. The same color indicates the same concentration of crowding agents. Error bars are the standard deviations from 1000 trajectories.

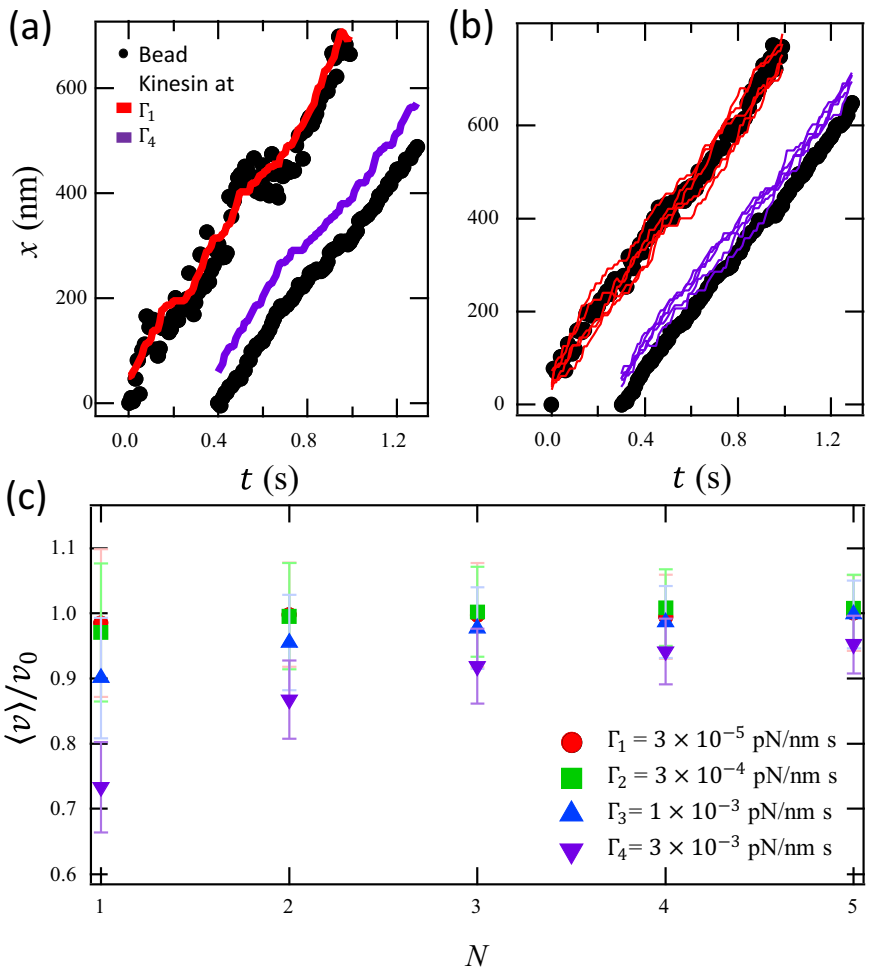

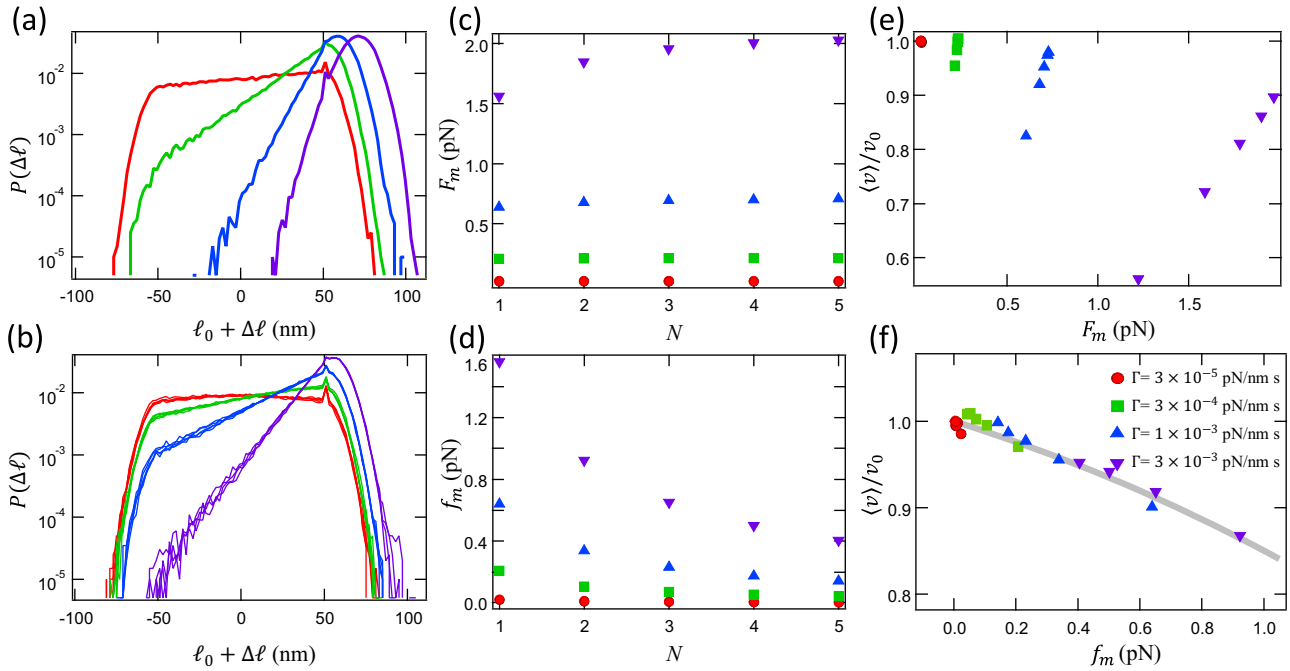

Fig. 6 | Kinesin stretching force in various crowder concentrations. The distribution of kinesin stretching (**a**) for $N = 1$ and (**b**) for $N = 5$ in various Γs. **c** Total force F_{mot} by multiple kinesins and (**d**) single motor force $f_{\mathrm{mot}} = F_{\mathrm{mot}}/N_{\mathrm{mot}}$ acting on cargo by N_{mot} kinesins for various crowding concentrations. Panels (**e**, **f**) Cargo velocities dependent of F_{mot} and f_{mot}.

concentration situation, that is, the load on a single kinesin is lower. We also examine the force, $F_m \equiv \sum_{j=1}^{N} K_j \Delta\ell_j$, acting on the cargo by multiple motors (Fig. 6c) and the force $f = F/N$ exerted by a single kinesin (Fig. 6d). Although the force F_m of the total number of motors increases as N increases, force per motor, f_m, decreases with N, indicating that the load on a single kinesin is reduced with more motors. This is even more dramatic for high-drag situations. Figure 6e, f presents $\langle v\rangle/v_0$ against F_m and f_m, respectively. They agree well with the experimental result in Fig. 3.

Discussion

In our study, we measured the velocity of the cargo transported by various numbers of kinesins in solutions with different molecular sizes and found two tendencies of velocity that vary with the number of kinesins involved. In small-crowder solutions, such as BSA or glycerol, the cargo velocity is lower than that in a solution without any crowders, regardless of the number of kinesins. This can be rationalized by the argument that small crowders directly affect the kinesin motion[20,21]. In contrast, larger crowders (Xanthan gum) cannot directly affect kinesin motion; they interact only with the cargo. Cargo velocity increases with the increasing number of kinesins, which agrees well with previous results[18,19]. The mean drag force exerted by a single kinesin or the force exerted by a single kinesin stretching collapses into a single curve of the cargo velocity carried by a single motor under external force (solid lines in Figs. 3b and 6f), indicating that the kinesins share the load on the cargo to move faster. Our finding seems to contradict the report that multiple kinesins are unable to generate force against the applied load cooperatively[8,36]. However, other studies in cells argue that it is possible for them to share the load on the cargo and thus increase the velocity of the cargo[37]. The discrepancy between these studies may be due to the degree of the crowdedness of the surrounding medium.

The exact mechanism of how multiple kinesins move collectively is still being explored, but the tension in the stalk might also play a role in coordinating the movement of multiple kinesins. Tjoe et al. focused on the intricate interplay between kinesin tension and cargo velocity in gliding assay experiments[28]. They suggested a scenario in which some kinesins actively pull the cargo forward while others resist this movement, creating a constant "tug-of-war" of tension, which plays a critical role in regulating cargo velocity in a crowded environment. Our finding also indicates that the tension due to the stretching of the kinesin results in load sharing. Kinesins may communicate with other kinesins attached to the same cargo through the tension of the stalk domain. Let us imagine that all kinesins are fully stretched. Then, one kinesin takes a step, which releases the tension of other kinesins and increases the possibility of others taking steps. This creates a cooperative effect.

Here, we note that although cargo hauled by multiple motors in crowded environments shows a broader velocity distribution in vitro than that by a single kinesin, it is still narrower than the cargo velocity distributions in cells. This suggests there are other factors that influence the complexity of intracellular transport. These include diverse kinesin motor types with varying speeds, microtubule heterogeneity, cargo-specific regulation via adaptor proteins, cellular crowding and obstacles impacting movement, and dynamic cellular signaling pathways modulating kinesin activity. Further in vitro experiments taking into these factors may provide a better understanding of the molecular motor's function within the crowded cellular environment.

In summary, this study demonstrated how the fluctuation theorem can be used to extract the number of motors instantaneously moving a cargo, and sheds light on the intricate interplay between proteins, crowders, and cargo transport. Our findings provide a deeper understanding of how molecular motors function under crowded conditions. Moreover, kinesin stalk tension is a fascinating aspect of these molecular motors. It contributes to the remarkable ability of multiple kinesins to work together and share the load, ensuring efficient and powerful cargo transport within cells.

Materials and methods

Kinesin purification

Tail-truncated kinesin-1 proteins (a human ubiquitous kinesin-1, KIF5B) were purified from bacteria as previously described in ref. 38. Escherichia coli BL21 (DE3) was transformed with the expression plasmid construct, and protein expression was induced with 0.1 mM IPTG. Cells were lysed by sonication (Branson SFX250), and the supernatant was collected by centrifugation of 28,000 g for 30 min. The supernatant was incubated with Ni-

NTA agarose (Qiagen Inc.) and eluted with 500 mM imidazole from a disposable column. The elution was subjected to dialysis to remove imidazole. Kinesin was further purified by microtubule affinity to remove inactive motor proteins. The proteins were incubated with taxol-stabilized microtubules and 1 mM AMP-PNP and were centrifuged at 200,000 g for 10 min. Active kinesin motors were released from microtubules by resuspension in a buffer containing 200 mM KCl and 5 mM ATP, and the supernatant was collected after centrifugation.

Motility assay

Kinesin was incubated with carboxylated polystyrene beads (490 nm, Polysciences, Warrington, PA) in 50 mL bead motility buffer (80 mM PIPES, pH 6.9, 50 mM CH3CO2K, 4 mM MgSO4, 1 mM dithiothreitol, 1 mM EGTA, 10 mM taxol, and 1 mg/mL casein) supplemented with 1 mM ATP for 15 min at room temperature. The kinesin assay buffer contains Xanthan gum (Xanthomonas campestris, Sigma, G1253), BSA (Sigma-Aldrich, A3059), or glycerol to increase the crowdness of the medium.

Taxol-stabilized microtubules (MT) were polymerized by incubating 12 μM tubulin (Cytoskeleton, Cat. TL240) in MT buffer (100 mm PIPES, 1 mm MgCl2, pH 6.9, 22 μM taxol, and 1.1 mM GTP) for 20 min at 37 °C, and incubated 5 μl tubulin (10 mg/ml) with 1.4 μl MT buffer at 37 °C for 30 minutes to polymerize MT (10 mg/ml). MT was diluted 200 times in DBMT buffer (35 mM PIPES, 5 mM MgSO4, 1 mM EGTA, 0.5 mM EDTA, 0.9 μl 10 mM Taxol) supplemented with 10 μl 10 mM GTP (Sigma, G8877).

All experiments are carried out in flow channels of 5 mm width and 100 μm depth, glued by double-sided tape between a glass slide and a glass coverslip precleaned with 0.1 M KOH solution. MTs were infused into the flow channel to be immobilized parallel to each other on the surface of the coverslip coated by poly-l-lysine (Sigma-Aldrich, P8920). After kinesin-bound beads were injected into the flow channel, the flow channel was sealed with nail polish. All procedures were carried out at room temperature.

Microscope system with optical tweezers

Optical tweezers were used to trap and move the particle close to MT. A 980 nm single mode fiber coupled diode laser (Thorlabs, BL976-SAG300) is focused in the sample plane of an optical microscope (Olympus IX73) through a 100X oil immersion objective lens (Olympus, UPLFN100XO, NA=1.3) to create the gradient force to trap a particle. The trapping force of the optical tweezers was measured by the position-sensitive device (DL100-7-PCBA3, Pacific Silicon Sensor, Thousand Oaks, CA). The trap stiffness is calibrated by two methods based on the equipartition theorem and the power spectrum[22]. During the experiment, we maintained stiffness small enough to allow the kinesins to escape the trap and walk freely along MT.

The movement of beads dragged by kinesins along the microtubules was visualized by differential interference contrast microscopy combined with optical tweezers and recorded with an sCMOS camera (pco.edge 3.1) at the frame rate of 100 Hz. The position of the particle was determined by our homemade tracking software, which was written in LabVIEW. After identifying the particle's positions, we transformed the coordinates of the trajectories to align the trajectory onto a single axis so that the particle's direction was parallel to the x-axis.

Xanthan buffer solution

Xanthan gum is a widely used water-soluble high molecular-weight polysaccharide ranging from 2×10^6 to 2×10^7 Da. In its native form, xanthan is probably double-stranded and is about as stiff as DNA. Due to these properties, xanthan gum shows excellent pseudoelasticity, thickening, and rheological properties and is highly stable to heat, acid, and alkali[39].

For this experiment, we prepared the master Xanthan solution, as described in ref. 19. Briefly, Xanthan gum, derived from Xanthomonas campestris (Sigma, G1253), was dissolved in Milli-Q water. Undissolved polymers and cellular debris were removed by centrifugation and filtered through a 0.45 μm syringe filter (Vivaspin 500, 30,000 MWCO PES). The filtered solution underwent dialysis against 80 mM PIPES buffer supplemented with 1 mM EGTA at pH 7.0. The final purified xanthan gum stock solution was stored at 5 °C for further use. In our experiments, we diluted the master Xanthan solution in kinesin buffer from 20% to 60%. The drag coefficients were determined from the measurement of the mean square displacement of 500 nm beads suspended at various concentrations of xanthan gum, as shown in Fig. 1a.

Measurement of the drag coefficient

To determine the drag coefficient of the Xanthan solution, we performed single-particle tracking experiments with 500 nm carboxylated particles. We recorded the particles at 1 μm away from the surface. To determine the drag coefficient Γ, we used the 1 μm magnetic beads that stay longer in the focal plane. Supplementary Fig. 1a shows the representative trajectories of particles near the surface of the coverslip for three concentrations of Xanthan of 20% (yellow), 40% (green), and 60% (purple). From the trajectories of the free diffusion particles, we estimated the two-dimensional mean square displacement. It is well-known that Brownian beads in non-desorbing polymer solution are surrounded by a layer depleted of polymer chains, which induces two different scales of diffusion, called a walking confined diffusion[40,41]. It is composed of long-term random diffusion and short-term confined diffusion, and the corresponding two-dimensional MSD can be written as follows.

$$\left\langle [\Delta r(t)]^2 \right\rangle = 4D_M t + 4D_m \tau (1 - e^{t/\tau}) \tag{5}$$

where $\Delta r(t)$ is the displacement in two dimensions, τ is the characteristic equilibrium time, and D_M and D_m are the long- and short-time diffusion constants, respectively. Supplementary Fig. 1b shows the measured MSD for various Xanthan concentrations, XC. As XC increases, the slope of the MSD ($4D_M$) for $t \gg \tau$ decreases. The drag coefficients were computed with the Stokes-Einstein relation, $\Gamma_0 = k_B T/D_M$.

However, these values are underestimated because, during kinesin walking, the particles are close to the surface, which increases the effective viscosity. So, we need to correct it. According to the Faxen's law[42], the relation between the viscosity near the surface Γ and that far from the surface Γ_0 is as follows:

$$\Gamma \approx \frac{\Gamma_0}{1 - \frac{9}{16}\frac{R}{s} + \frac{1}{8}\left(\frac{R}{s}\right)^3}, \tag{6}$$

where R is the radius of the particle, and s is the distance between the center of the particle and the surface. We measured Γ at s=2 μm and corrected it for s=50 nm. Then, we obtained the effective Γ for the kinesin experiment, as shown in Fig. 1a.

The recorded data were analyzed by Igor Pro software; the velocity of the movement was calculated through a linear curve fitting between the binding point at the detachment. Data for each bead were collected separately. The processivity histograms (travel distance between attachment and diffusion), binding time, and velocity were then extracted from the collective data. The average values and standard deviations were obtained by fitting the exponential decaying or Gaussian distribution to the histograms.

Theoretical model for counting the number of motors using fluctuation theorem

To study the cargo motion hauled by multiple kinesin motors, identification of the number of motors actively involved in cargo motion is essential. As a non-invasive way, Hayashi et al. developed the technique using the fluctuation theorem[24,25,43] with the concept of the effective temperature[44,45]. The following is a brief description of how to apply for it.

Assuming that a cargo carried by kinesin-1 motors moves toward the plus-end of the microtubule, the motion of the cargo is described by the overdamped Langevin equation:

$$\Gamma \frac{dx_p}{dt} = -\frac{\partial U_m(x_p, t)}{\partial x_p} + \xi(t), \tag{7}$$

where $x_p(t)$ is a cargo position, and $\Gamma = 6\pi\eta R$ is the drag coefficient of the cargo (η is the viscosity of medium and R is a radius of a cargo). Thermal force $\xi(t)$ has a zero mean and variance $\langle \xi(t)\xi(t')\rangle = 2\Gamma k_B T\delta(t-t')$ with the Boltzmann constant k_B and the environment temperature T. $U_m(x, t)$ is the potential energy of the interaction between cargo and motors.

The fluctuation theorem for the non-equilibrium steady state is expressed as the ratio of the probability of the positive entropy production rate (denoted by $\dot{\mathcal{S}}$) to that of the negative entropy production rate ($-\dot{\mathcal{S}}$), which is equal to an exponential function of $\dot{\mathcal{S}}\Delta t/k_B$, where Δt is the duration of the measurement. It is written as

$$\frac{P_{\Delta t}(\dot{\mathcal{S}})}{P_{\Delta t}(-\dot{\mathcal{S}})} = e^{\frac{\dot{\mathcal{S}}\Delta t}{k_B}}. \tag{8}$$

The fluctuation theorem has been experimentally verified and applied to biological systems[46,47]. For example, Hayashi et al. used the fluctuation theorem to estimate the rotary torque of F_1-ATPase[48].

As kinesin walks along MT by hydrolyzing ATP, it changes its conformation to move a step. The heat change of the entropy production rate in FT is presented in the form of a generated work in the kinesin working function. Thus, we replace the entropy production in a duration of Δt, $\dot{\mathcal{S}}\Delta t$ with the work W, and hence $\dot{\mathcal{S}}T\Delta t = W = F_m\Delta x_p$. $F_m\Delta x_p$ is the stochastic work done by kinesin, and $\Delta x_p(\Delta t) = x_p(t+\Delta t) - x_p(t)$. Therefore, the fluctuation theorem for the kinesin motion reads:

$$\frac{P\left(\Delta x_p\right)}{P\left(-\Delta x_p\right)} = \exp\left[\frac{F_m\Delta x_p}{k_B T}\right]. \tag{9}$$

From this relation, we can define the degree of fluctuation χ[23,43] as:

$$\frac{F_m}{k_B T} = \ln\left[\frac{P\left(\Delta x_p\right)}{P\left(-\Delta x_p\right)}\right]/\Delta x_p \equiv \chi. \tag{10}$$

To observe a broad range of fluctuations in the macroscopic scale, we vary Δt to probe the trend of χ. If $P(\Delta x_p)$ is fitted by Gaussian distribution well,

$$P(\Delta x_p) = \frac{1}{\sqrt{2\pi\sigma^2}}\exp\left(-\frac{\left(\Delta x_p-\mu\right)^2}{2\sigma^2}\right), \tag{11}$$

we can simplify χ as

$$\chi = 2\mu/\sigma^2. \tag{12}$$

Here, Δt is the time lag, and $\mu = \langle\Delta x_p\rangle$ and $\sigma = \langle(\Delta x_p - \langle\Delta x_p\rangle)^2\rangle$ are the mean and the variance of the distribution, respectively.

In a small time scale (small Δt) but still larger than the relaxation time τ_R, the dominating fluctuations make the mean displacement $\langle\Delta x_p\rangle$ close to zero, leading χ is small. As Δt increases, the directional transport of cargo becomes dominant so that χ increases and gradually converges to a fixed value. That is, a larger Δt causes the friction force ($\Gamma dx_p/dt$) to be closer to the kinesin force F_m in Eq. (9). We denote the convergent χ by χ^* :

$$\lim_{t\to\infty}\frac{F_m}{k_B T} = \chi^*. \tag{13}$$

Hence, the kinesin force is proportional to χ^* and is assumed to be proportional to the number of motors. Therefore, χ^* gives an indicative value to identify the number of active motors tethered to the bead involved in transport. An alternative explanation is given by Peng et al.[26]. Assuming the distribution is Gaussian, they confirmed that the peaks in χ^* are equally spaced and correspond to the number of motors.

Simulation of a two-state model of kinesin

Simulations of kinesin motor walking on the microtubule were performed using the Monte Carlo approach based on the two-state model. The transition rate from state 1 to state 2 is k_c, and the transition rates to make a forward or backward step in the stepping state are k_f and k_b, respectively. Here, k_f and k_b have an Arrhenius-type force dependency. The motor makes a forward or backward step of length d (8 nm), and the cargo has a damping coefficient of Γ. Here, we consider that the kinesin motor is attached to the cargo and attempts to move in the positive x direction. Let the instantaneous position of the cargo be $x_p(t)$, and let the head and tail positions be denoted by $x_p(t) + \delta$ and $x(t)$, respectively (see Fig. 4b). The motor is attached to the particle by a spring of stiffness K. The intrinsic force-free size of the spring is denoted by ℓ_o. The equations of motion are

$$\Gamma\dot{x}_p = -K\Delta\ell + F_{load} + \xi_p(t), \tag{14}$$

where $\Delta\ell \equiv x_p + \delta + \ell_o - x$ corresponds to the extension of the walking motor beyond its rest length l_0 (50 nm), F_{load} is the external force on cargo, and ξ_p is white Gaussian thermal fluctuations that satisfy $\langle\xi_p\rangle = 0$ and $\langle\xi_p(t)\xi_p(t')\rangle = 2\Gamma k_B T\delta(t-t')$. The forward or backward rate $k_{f,b}^{(j)}$ depends on the force experienced by the motor and is modeled by the Bell's equation:

$$k_{f,b} = k_{0f,b}e^{d_{f,b}K\Delta\ell/k_B T}, \tag{15}$$

where $d_{f,b}$ are some characteristic distances.

The simulations were conducted with Langevin dynamics of the cargo, which is connected to the kinetic kinesin model via an elastic linker, using Eq. (14). The parameters used in the numerical simulation are taken from ref. 35, such as k_c=1002s^{-1}, k_{0f}=102s^{-1}, k_{0b}=27.3s^{-1}. We also selected the stiffness of the kinesin stalk is 0.75×10^{-4} N/m, and the cargo radius is 250 nm. The time step of the simulation is $\Delta t = 10^{-1}$ s. The result is shown in Supplementary Fig. 2.

The corresponding mean velocity of cargo by a single kinesin under the load, F_{load}, is given as follows[34]:

$$\langle v\rangle = d\times\frac{(k_f-k_b)k_c}{k_f+k_b+k_c}. \tag{16}$$

The simulation is in good agreement with the theoretical prediction.

Statistics and reproducibility

For all statistical analyses, data were collected from five different concentrations of Xanthan gum, and cargo tracking data were obtained from at least ten different sets of experiments; specific sample sizes are in the text. Mean velocities were determined by fitting a Gaussian function to the velocity histograms, and error bars represent the standard deviation. In the numerical simulations, 1000 tracks generated from a single simulation were analyzed for each condition. All statistical analyses were performed using Igor Pro software.

Reporting summary

Further information on research design is available in the Nature Portfolio Reporting Summary linked to this article.

Data availability

The raw data for the graphs in Figs. 2g, 3, 5c, and 6c–f can be found in Supplementary Data 1. All other data are available from the corresponding author upon reasonable request.

Code availability

The code, written using Igor Pro software, is available at https://github.com/junlabtw/crowding or can be requested from the corresponding author.

Received: 24 September 2024; Accepted: 17 January 2025;
Published online: 13 February 2025

References

1. Gross, S. P., Welte, M. A., Block, S. M. & Wieschaus, E. F. Coordination of opposite-polarity microtubule motors. *Journal Cell Biology* **156**, 715–724 (2002).
2. Hirokawa, N., Noda, Y., Tanaka, Y. & Niwa, S. Kinesin superfamily motor proteins and intracellular transport. *Nature Reviews. Molecular Cell Biology* **10**, 682–96 (2009).
3. Veigel, C. & Schmidt, C. F. Moving into the cell: single-molecule studies of molecular motors in complex environments. *Nature Reviews. Molecular Cell Biology* **12**, 163–76 (2011).
4. Svoboda, K., Schmidt, C. F., Schnapp, B. J. & Block, S. M. Direct observation of kinesin stepping by optical trapping interferometry. *Nature* **365**, 721–727 (1993).
5. Brady, S. T., Lasek, R. J. & Allen, R. D. Fast axonal transport in extruded axoplasm from squid giant axon, Fast Axonal Transport in Squid Giant Axon Abstract. *Science* **218**, 1129–1131 (1982).
6. Smith, G. A., Gross, S. P. & Enquist, L. W. Herpesviruses use bidirectional fast-axonal transport to spread in sensory neurons. *Proceedings National Academy Sciences USA* **98**, 3466–3470 (2001).
7. Shubeita, G. T. et al. Consequences of motor copy number on the intracellular transport of kinesin-1-driven lipid droplets. *Cell* **135**, 1098–107 (2008).
8. Furuta, K. et al. Measuring collective transport by defined numbers of processive and nonprocessive kinesin motors. *Proc. Natl Acad. Sci*. **110**, 501–506 (2012).
9. Derr, N. D. et al. Tug-of-War in Motor Protein Ensembles Revealed with a Programmable DNA Origami Scaffold. *Science* **338**, 662–665 (2012).
10. Xu, J., King, S. J., Lapierre-Landry, M. & Nemec, B. Interplay between velocity and travel distance of Kinesin-based transport in the presence of tau. *Biophysical Journal* **105**, L23–L25 (2013).
11. Ellis, R. J. Macromolecular crowding: obvious but underappreciated. *Trends Biochemical Sciences* **26**, 597–604 (2001).
12. Zhou, Huan-Xiang, Rivas, Germán & Minton, A. P. Macromolecular crowding and confinement: Biochemical, biophysical, and potential physiological consequences*. *Annual Review Biophysics* **37**, 375–397 (2008).
13. Totani, K., Ihara, Y., Matsuo, I. & Ito, Y. Effects of macromolecular crowding on glycoprotein processing enzymes. *Journal American Chemical Society* **130**, 2101–2107 (2008).
14. Dhar, A. et al. Structure, function, and folding of phosphoglycerate kinase are strongly perturbed by macromolecular crowding. *Proceedings National Academy Sciences* **107**, 17586–17591 (2010).
15. Chiba, K. et al. Quantitative analysis of APP axonal transport in neurons: Role of JIP1 in enhanced APP anterograde transport. *Molecular Biology Cell* **25**, 3569–3580 (2014).
16. Theos, A. C. et al. Functions of adaptor protein (AP)-3 and AP-1 in tyrosinase sorting from endosomes to melanosomes. *Molecular Biology Cell* **16**, 5356–5372 (2005).
17. Pilling, A. D., Horiuchi, D., Lively, C. M. & Saxton, W. M. Kinesin-1 and Dynein Are the Primary Motors for Fast Transport of Mitochondria in Drosophila Motor Axons. *Mol. Biol. Cell* **17**, 2057–2068 (2006).
18. Hunt, A. J., Gittes, F. & Howard, J. The force exerted by a single kinesin molecule against a viscous load. *Biophysical Journal* **67**, 766–781 (1994).
19. Gagliano, J., Walb, M., Blaker, B., Macosko, J. C. & Holzwarth, G. Kinesin velocity increases with the number of motors pulling against viscoelastic drag. *European Biophysics Journal* **39**, 801–813 (2010).
20. Sozański, K. et al. Small Crowders Slow Down Kinesin-1 Stepping by Hindering Motor Domain Diffusion. *Physical Review Letters* **115**, 218102 (2015).
21. Nettesheim, G. et al. Macromolecular crowding acts as a physical regulator of intracellular transport. *Nature Physics* **16**, 1144–1151 (2020).
22. Jun, Y., Tripathy, S. K., Narayanareddy, BabuR. J., Mattson-Hoss, M. K. & Gross, S. P. Calibration of Optical Tweezers for In Vivo Force Measurements: How do Different Approaches Compare? *Biophys. J.* **107**, 1474–1484 (2014).
23. Hayashi, K., Hasegawa, S., Sagawa, T., Tasaki, S. & Niwa, S. Non-invasive force measurement reveals the number of active kinesins on a synaptic vesicle precursor in axonal transport regulated by ARL-8. *Physical Chemistry Chemical Physics* **20**, 3403–3410 (2018).
24. Hayashi, K. Application of the fluctuation theorem to motor proteins: from F1-ATPase to axonal cargo transport by kinesin and dynein. *Biophysical Reviews* **10**, 1311–1321 (2018).
25. Hasegawa, S., Sagawa, T., Ikeda, K., Okada, Y. & Hayashi, K. Investigation of multiple-dynein transport of melanosomes by non-invasive force measurement using fluctuation unit *χ*. *Scientific Reports* **9**, 5099 (2019).
26. Peng, C. et al. Nanometer-resolution tracking of single cargo reveals dynein motor mechanisms. *Nature Chemical Biology* **122**, 1a (2024).
27. Fallesen, T. L., MacOsko, J. C. & Holzwarth, G. Force-velocity relationship for multiple kinesin motors pulling a magnetic bead. *European Biophysics Journal* **40**, 1071–1079 (2011).
28. Tjioe, M. et al. Multiple kinesins induce tension for smooth cargo transport. *eLife* **8**, 1–31 (2019).
29. Papagiannopoulos, A. & Sklapani, A. Xanthan-based polysaccharide/protein nanoparticles: Preparation, characterization, encapsulation and stabilization of curcumin. *Carbohydrate Polymer Technologies Applications* **2**, 100075 (2021).
30. Smilgies, Detlef-M. & Folta-Stogniew, E. Molecular weight–gyration radius relation of globular proteins: a comparison of light scattering, small-angle X-ray scattering and structure-based data. *Journal Applied Crystallography* **48**, 1604–1606 (2015).
31. Jahn, D. A., Wong, J., Bachler, J., Loerting, T. & Giovambattista, N. Glass polymorphism in glycerol-water mixtures: I. A computer simulation study. *Physical Chemistry Chemical Physics* **18**, 11042–11057 (2016).
32. Svoboda, K. & Block, S. M. Force and velocity measured for single kinesin molecules. *Cell* **77**, 773–84 (1994).
33. Taniguchi, Y., Nishiyama, M., Ishii, Y. & Yanagida, T. Entropy rectifies the Brownian steps of kinesin. *Nature Chemical Biology* **1**, 342–347 (2005).
34. Ariga, T., Tomishige, M. & Mizuno, D. Nonequilibrium Energetics of Molecular Motor Kinesin. *Physical Review Letters* **121**, 218101 (2018).
35. Ariga, T., Tateishi, K., Tomishige, M. & Mizuno, D. Noise-Induced Acceleration of Single Molecule Kinesin-1. *Physical Review Letters* **127**, 178101 (2021).
36. Jamison, D. K., Driver, J. W., Rogers, A. R., Constantinou, P. E. & Diehl, M. R. Two kinesins transport cargo primarily via the action of one motor: implications for intracellular transport. *Biophysical Journal* **99**, 2967–77 (2010).
37. Reis, G. F. et al. Molecular motor function in axonal transport in vivo probed by genetic and computational analysis in Drosophila. *Molecular Biology Cell* **23**, 1700–14 (2012).
38. Isojima, H., Iino, R., Niitani, Y., Noji, H. & Tomishige, M. Direct observation of intermediate states during the stepping motion of kinesin-1. *Nature Chemical Biology* **12**, 290–297 (2016).
39. Palaniraj, A. & Jayaraman, V. Production, recovery and applications of xanthan gum by xanthomonas campestris. *Journal Food Engineering* **106**, 1–12 (2011).
40. Daumas, F. et al. Confined Diffusion Without Fences of a G-Protein-Coupled Receptor as Revealed by Single Particle Tracking. *Biophysical Journal* **84**, 356–366 (2003).
41. Ochab-Marcinek, A. & Hołyst, R. Scale-dependent diffusion of spheres in solutions of flexible and rigid polymers: mean square displacement and autocorrelation function for FCS and DLS measurements. *Soft Matter* **7**, 7366 (2011).
42. Leach, J. et al. Comparison of Faxén's correction for a microsphere translating or rotating near a surface. *Physical Review E* **79**, 1–4 (2009).
43. Hayashi, K., Tsuchizawa, Y., Iwaki, M. & Okada, Y. Application of the fluctuation theorem for noninvasive force measurement in living neuronal axons. *Molecular Biology Cell* **29**, 3017–3025 (2018).

44. Hayashi, K. & Sasa, Shin-ichi Effective temperature in nonequilibrium steady states of Langevin systems with a tilted periodic potential. *Physical Review E* **69**, 066119 (2004).
45. Hayashi, K. & Sasa, Shin-ichi Decomposition of force fluctuations far from equilibrium. *Physical Review E* **71**, 020102 (2005).
46. Wang, G. M., Sevick, E. M., Mittag, E., Searles, D. J. & Evans, D. J. Experimental Demonstration of Violations of the Second Law of Thermodynamics for Small Systems and Short Time Scales. *Phys. Rev. Lett.* **89**, 050601 (2002).
47. Feitosa, K. & Menon, N. Fluidized granular medium as an instance of the fluctuation theorem. *Phys. Rev. Lett.* **92**, 164301 (2004).
48. Hayashi, K., Ueno, H., Iino, R. & Noji, H. Fluctuation Theorem Applied to F_{1}-ATPase. *Phys. Rev. Lett.* **104**, 218103 (2010).

Acknowledgements

This work has been supported by the National Science and Technology Council of Taiwan under Grants No. 112-2112-M-008 -030- (Y.J.) and No. 113-2112-M-008-018-MY2 (P.Y.-L.).

Author contributions

Y.H. and Y.J. designed the experiment; Y.H. carried out the experiment; Y.H. and Y.J. analyzed the data; Y.J. and P.-Y.L. performed numerical simulation; Y.H., Y.J., M.T., S.P.G., and P.-Y.L. discussed and interpreted results, and wrote the manuscript.

Competing interests

The authors declare no competing interests.

Additional information

Supplementary information The online version contains supplementary material available at https://doi.org/10.1038/s42003-025-07573-3.

Correspondence and requests for materials should be addressed to Pik-Yin Lai or Yonggun Jun.

Peer review information : *Communications Biology* thanks Shinsuke Niwa and the other, anonymous, reviewer(s) for their contribution to the peer review of this work. Primary Handling Editor: Kaliya Georgieva.